Received: 12 March 2020 | Revised: 29 July 2020 | Accepted: 30 July 2020

DOI: 10.1002/mrm.28486

NOTE

Magnetic Resonance in Medicine

Segmented K-space blipped-controlled aliasing in parallel imaging for high spatiotemporal resolution EPI

Rüdiger Stirnberg[1] | **Tony Stöcker**[1,2]

[1]German Center for Neurodegenerative Diseases (DZNE), Bonn, Germany

[2]Department of Physics and Astronomy, University of Bonn, Bonn, Germany

Correspondence
Rüdiger Stirnberg, German Center for Neurodegenerative Diseases (DZNE), Venusberg-Campus 1, Building 99, D-53127 Bonn, Germany.
Email: ruediger.stirnberg@dzne.de

Purpose: A segmented k-space blipped-controlled aliasing in parallel imaging (skipped-CAIPI) sampling strategy for EPI is proposed, which allows for a flexible choice of EPI factor and phase encode bandwidth independent of the controlled aliasing in parallel imaging (CAIPI) sampling pattern.

Theory and Methods: With previously proposed approaches, exactly two EPI trajectories were possible given a specific CAIPI pattern, either with slice gradient blips (blipped-CAIPI) or following a shot-selective CAIPI approach (higher resolution). Recently, interleaved multi-shot segmentation along shot-selective CAIPI trajectories has been applied for high-resolution anatomical imaging. For more flexibility and a broader range of applications, we propose segmentation along any blipped-CAIPI trajectory. Thus, all EPI factors and phase encode bandwidths available with traditional segmented EPI can be combined with controlled aliasing.

Results: Temporal SNR maps of moderate-to-high-resolution time series acquisitions at varying undersampling factors demonstrate beneficial sampling alternatives to blipped-CAIPI or shot-selective CAIPI. Rapid high-resolution scans furthermore demonstrate SNR-efficient and motion-robust structural imaging with almost arbitrary EPI factor and minimal noise penalty.

Conclusion: Skipped-CAIPI sampling increases protocol flexibility for high spatiotemporal resolution EPI. In terms of SNR and efficiency, high-resolution functional or structural scans benefit vastly from a free choice of the CAIPI pattern. Even at moderate resolutions, the independence of sampling pattern, TE, and image matrix size is valuable for optimized functional protocol design. Although demonstrated with 3D-EPI, skipped-CAIPI is also applicable with simultaneous multislice EPI.

KEYWORDS

3D-EPI, blipped-CAIPI, CAIPIRINHA, EPI, interleaved multi-shot, segmented EPI

1 | INTRODUCTION

An increasing number of structural imaging,[1-6] quantitative imaging,[7-10] or high spatiotemporal resolution functional imaging[11-21] applications have been approached by dedicated EPI[22] implementations. Many of those aim at higher spatial resolution than usual, for example, in fMRI. It is generally appealing to combine the inherent SNR efficiency of EPI[23,24] with the controlled aliasing in parallel imaging results in higher acceleration (CAIPIRINHA, short: CAIPI[25]) technique to minimize the geometry-dependent parallel imaging noise penalty (g-factor[26]). However, previous sampling approaches limit each CAIPI pattern to only two possible EPI k-space trajectories and corresponding EPI factors: single-shot blipped-CAIPI[27] and multi-shot shot-selective CAIPI.[18,28,29] Thus, higher-priority parameters affecting the EPI factor as well (eg, base resolution and TE) often enforce a suboptimal CAIPI pattern instead of a noise-optimal one. Recently, shot-selective CAIPI has been combined with interleaved multi-shot segmentation fostering rapid T_1-weighted anatomical imaging.[6] Still, this approach is limited to only a fraction of traditional segmentation options without controlled aliasing. We demonstrate that introducing a segmentation factor into blipped-CAIPI overcomes these limitations and proves useful for a wide range of high spatiotemporal resolution applications.

2 | THEORY

2.1 | Segmented EPI

Interleaved multi-shot segmentation has been proposed very early to achieve higher resolutions with reduced off-resonance artifacts (eg, geometric distortions, chemical shift) and T_2^*-related artifacts ("T_2^* blur"), shorter TEs, and repetition times per shot (TR).[30] Parallel imaging along the blipped phase encode direction (y, without loss of generality) also helps with this regard: combined with S-fold segmentation, the phase encoding y -blip becomes $S \cdot R_y$, compared to only R_y (undersampling factor along y) without segmentation. The y-blip directly controls the EPI factor, $EF = \lceil N_y / S \cdot R_y \rceil$, and the phase encode bandwidth, $BW_y = S \cdot R_y / ESP$, where N_y and ESP denote the phase encode matrix size and the echo spacing, respectively. Echo time shifting can be introduced to smooth out signal magnitude and phase jumps between adjacent odd-/even-echo k-space sections.[31,32] The segmentation technique has been combined with 3D-EPI and with parallel imaging along two directions (Figure 1A), for example, for T_2^*/susceptibility-weighted high-resolution imaging[1,2] or fMRI,[13-15,17,19,33] but these implementations lacked controlled aliasing.

2.2 | Blipped-CAIPI

Simultaneous multislice (SMS) EPI[27] or 3D-EPI using blipped-CAIPI sampling[16,20,34-36] can employ stronger undersampling owing to a reduced g-factor. Positive and negative gradient blips along the slice or secondary phase encode axis (z, without loss of generality) are introduced between echoes along the EPI train, resulting in a certain CAIPI sampling pattern

$$R_y \times R_{z\,\Delta z}.$$

Here, R_z and Δz denote the undersampling (multiband) factor and the CAIPI shift along z, respectively. The same pattern can also be expressed with a CAIPI shift along y. The z-notation[37] is adopted here with $-\lfloor R_z/2 \rfloor \le \Delta z \le \lfloor R_z/2 \rfloor$. Generally, selecting an adequate CAIPI pattern minimizes the g-factor in the fundamental relation[26]:

$$SNR = \frac{SNR_0}{g\sqrt{R}}. \quad (1)$$

SNR_0 is the volumetric SNR without undersampling and

$$R = R_y \cdot R_z$$

is the total undersampling factor. For SMS-EPI, $SNR_0 = SNR_{\text{slice}}\sqrt{R_z}$ is often inserted into Equation 1, where SNR_{slice} is the single-slice SNR without undersampling. Either way, each CAIPI pattern corresponds to one unique blipped-CAIPI trajectory. In z-notation, the y-blip is exactly R_y (Figure 1, row 1).

2.3 | Shot-selective CAIPI

At high spatiotemporal resolutions, it has been proposed to first acquire only those samples of the CAIPI pattern in a single shot that correspond to one secondary phase encode value. In the next shot, all samples that correspond to the next secondary phase encode value of the CAIPI pattern are acquired, etc.[28,29] Such a shot-selective CAIPI approach has recently been applied with SMS-EPI[5] and 3D-EPI[18] to achieve greater y-blips. Each CAIPI pattern corresponds to one unique shot-selective trajectory without z-blips. The y-blip is exactly R_z times larger than that of the blipped-CAIPI trajectory for the same CAIPI pattern (Figure 1B, row 2), unless the z-CAIPI shift is a factor of R_z; in that case, the shot-selective y-blip is only $R_z/|\Delta z|$ times larger than the blipped-CAIPI y-blip (Figure 1C, row 2).

3 | METHODS

Segmentation can be applied along the shot-selective CAIPI trajectory to achieve even larger y-blips as a multiple of the

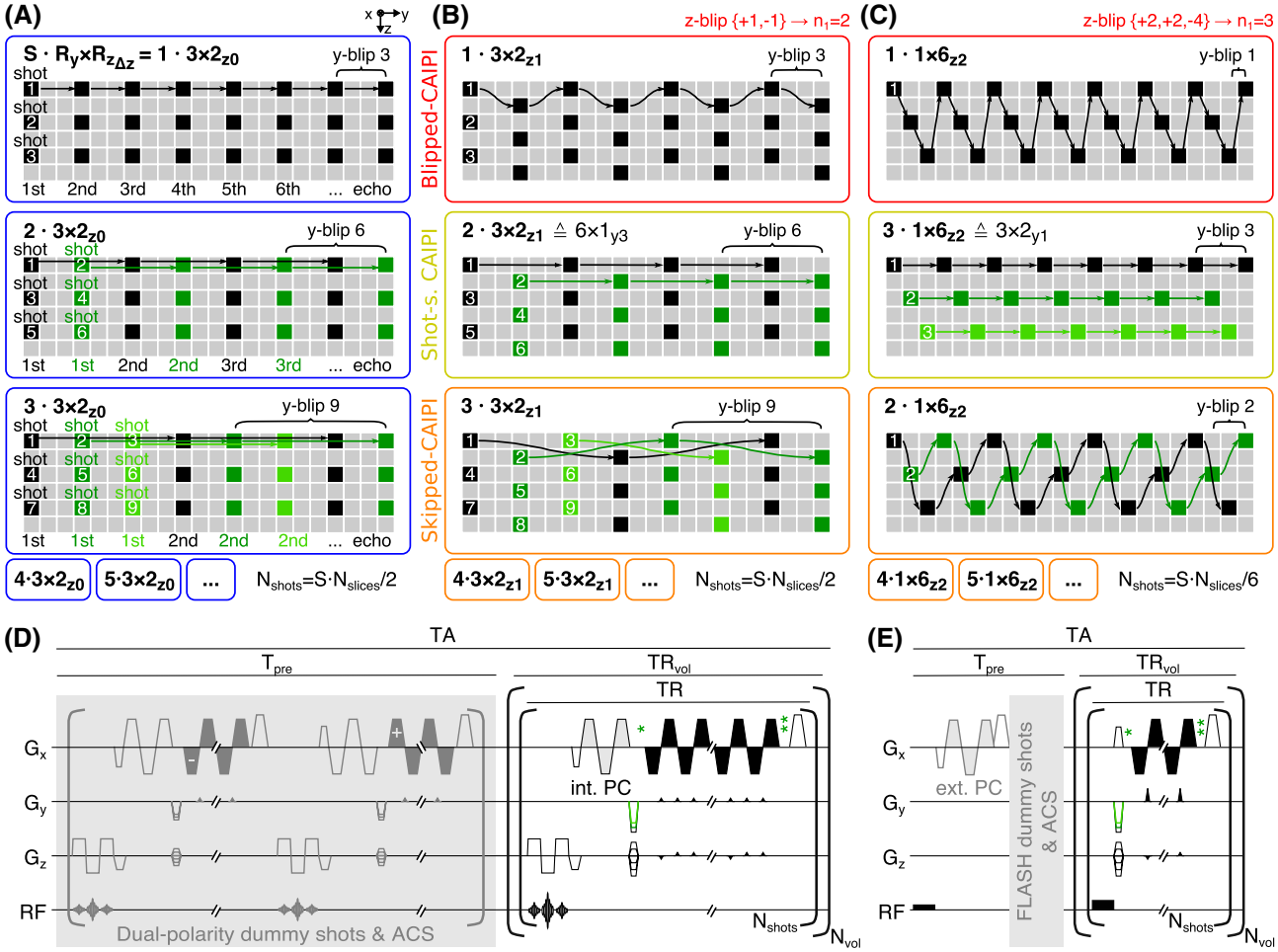

FIGURE 1 Schematic depiction of traditional (segmented) 3D-EPI k-space sampling with 3 × 2 undersampling (A) and derived CAIPI trajectories for the corresponding $3 \times 2_{z_1}$ CAIPI pattern (B) and for an alternative $1 \times 6_{z_2}$ CAIPI pattern (C). Rows 1 and 2: the blipped-CAIPI and the shot-selective CAIPI trajectory for the respective pattern. Row 3: 1 skipped-CAIPI trajectory example. (D and E) Schematic diagram of slab-selective (oblique-axial time series) and whole-head (sagittal high-resolution) sequence variants used here. Pre-(*)/post-(**)-EPI delay times increase/decrease with the first primary phase encode value per shot for echo time shifting (see Supporting Information Figure S8 for visualization). ACS, autocalibration scan; CAIPI, controlled aliasing in parallel imaging; $N_{shots} = S{\cdot}N_{slices}/R_z$, number of shots per volume measurement; N_{slices}, number of slices; N_{vol}, number of volume measurements; PC, phase correction scan.

shot-selective *y*-blip.[6] In this work, we go one step further and propose segmentation along the blipped-CAIPI trajectory to also obtain all intermediate *y*-blips and *EF*s. This segmented k-space blipped-CAIPI (skipped-CAIPI) approach maximally unlinks the *y*-blip from the CAIPI pattern. Skipped-CAIPI is demonstrated on the example of a 3D-EPI sequence. However, it can be applied to SMS-3D k-space without loss of generality.[38-40]

3.1 | Skipped-CAIPI

A skipped-CAIPI sampling trajectory is defined by the CAIPI pattern and a segmentation factor, $S \geq 1$. Along the blipped-CAIPI trajectory, $S - 1$ echoes are skipped and acquired in subsequent shots (Figure 1, row 3). Analogous to segmented EPI, the *y*-blip becomes $S \cdot R_y$. In fact, traditional segmented EPI corresponds to skipped-CAIPI with $\Delta z = 0$ (Figure 1A). Blipped-CAIPI corresponds to skipped-CAIPI with $\Delta z \neq 0$ and $S = 1$ (Figure 1B-C, row 1). The CAIPI pattern is not affected by the segmentation factor. For the sampling trajectory, we use the shorthand notation:

$$S \cdot R_y \times R_{z\,\Delta z}.$$

Like blipped-CAIPI, most skipped-CAIPI trajectories imply *z*-blips between echoes. Two *z*-blips with opposed polarity are repeated in a sequential order with a certain cycle. The *z*-blip cycle of blipped-CAIPI is $n_1 = R_z$ (eg, Figure 1B, row 1), unless Δz is a factor of R_z, which results in $n_1 = R_z / |\Delta z|$ (eg, Figure 1C, row 1). Consequently, employing skipped-CAIPI with $S = n_1$ equals shot-selective CAIPI (Figure 1B-C, row 2). Although $S = 2n_1, 3n_1, \ldots$ trajectories may be considered "segmented shot-selective," we refer to

them as "skipped-CAIPI without *z*-blips" to avoid ambiguity. For more details, we refer the reader to the Appendix.

Like segmented EPI, skipped-CAIPI hypothetically works for all S up to N_y/R_y even though very large S are not efficient. Given a CAIPI pattern, $1/n_1$ of all corresponding trajectories do not imply *z*-blips, including shot-selective CAIPI ($S = n_1$). An equal or greater number, $(n_1 - 1)/n_1$ of all trajectories, implies *z*-blips including blipped-CAIPI ($S = 1$). See Supporting Information Figure S1 for a plot of *EF* versus *y*-blip, and S2 for a graphical representation of all sampling trajectories with identical *z*-blips for the same three CAIPI pattern examples. This demonstrates the utility of skipped-CAIPI if a g-factor-optimal CAIPI pattern is selected first, and the segmentation factor is adjusted thereafter to achieve a specific *EF*, TE, TR, BW_y, and so forth (eg, structural MRI protocols). Vice versa, if the *y*-blip shall have a fixed value, Supporting Information Figures S3-S5 show all possible CAIPI patterns up to $R = 8$ according to Ref. 37, as well as sampling trajectories that yield a *y*-blip of 2, 3, and 4. This demonstrates the utility of skipped-CAIPI if the experiment requires a specific *EF*, TE, or *y*-blip, and so forth: the best CAIPI pattern that fulfils this requirement at any acceleration factor can now be selected, whereas previously only limited acceleration factors and potentially suboptimal CAIPI patterns were possible (eg, functional MRI protocols).

3.2 | Experiments

All experiments were performed on a 3 Tesla Magnetom Skyra version VE11C (Siemens Healthineers, Erlangen, Germany) equipped with a 45 mT/m, 200 T/m/s gradient system and a 32-channel head coil. A custom RF-spoiled 3D-EPI sequence with echo time shifting was used (Figure 1D-E).

One healthy male subject was scanned after providing informed consent in accordance with local institutional review board regulations. Two protocol types tailored toward whole-brain fMRI (Table 1) and rapid T_1-weighted structural imaging were used (Table 2). All images were reconstructed using a generic vendor-preinstalled GRAPPA[41] implementation compatible with 2D CAIPIRINHA[37] (IcePAT) in conjunction with the vendor-default phase correction and ramp-sampling implementation.

TABLE 1 Sampling trajectories and sequence parameters for time series EPI acquisitions using small y-blips

		y-blip 2	y-blip 3	y-blip 4
R		**CAIPI sampling trajectory (N_{shots} / TR_{vol})**		
4	Blipped	$1\cdot2\times2_{z1}$ (36/1.90 s)	N/A	N/A
	Shot-s.	$2\cdot1\times4_{z2}$ (36/1.90 s)	N/A	$2\cdot2\times2_{z1}$ (80/4.70 s)
	Skipped	$2\cdot1\times4_{z1}$ (36/1.90 s)	$3\cdot1\times4_{z2}$ (60/3.5 s)	$4\cdot1\times4_{z2}$ (80/4.70 s)
5	Skipped	$2\cdot1\times5_{z2}$ (28/1.48 s)	$3\cdot1\times5_{z2}$ (48/2.8 s)	$4\cdot1\times5_{z2}$ (64/3.80 s)
6	Blipped	$1\cdot2\times3_{z1}$ (24/1.26 s)	$1\cdot3\times2_{z1}$ (42/2.5 s)	N/A
	Shot-s.	$2\cdot1\times6_{z3}$ (24/1.27 s)	$3\cdot1\times6_{z2}$ (42/2.5 s)	N/A
	Skipped	$2\cdot1\times6_{z2}$ (24/1.28 s)	$3\cdot1\times6_{z3}$ (42/2.5 s)	$4\cdot1\times6_{z2}$ (56/3.30 s)
7	Skipped	$2\cdot1\times7_{z2}$ (20/1.07 s)	$3\cdot1\times7_{z2}$ (36/2.1 s)	$4\cdot1\times7_{z2}$ (48/2.90 s)
8	Blipped	$1\cdot2\times4_{z2}$ (18/0.95 s)	N/A	$1\cdot4\times2_{z1}$ (40/2.40 s)
	Shot-s.	$2\cdot1\times8_{z4}$ (18/0.95 s)	N/A	$2\cdot2\times4_{z2}$ (40/2.40 s)
	Skipped	$2\cdot1\times8_{z2}$ (18/0.97 s)	$3\cdot1\times8_{z2}$ (30/1.75 s)	$4\cdot1\times8_{z3}$ (40/2.40 s)
	EF	54	48	45
	Res.	2 mm isotropic	1.5 mm isotropic	1.2 mm isotropic
	Matrix	108 × 108	144 × 144	180 × 180
	N_{slices}	72 (70 for R = 5, 7)	80 (84 for R = 6, 7)	80 (84 for R = 6, 7)
	BW_x	1714 Hz/pixel	1240 Hz/pixel	1112 Hz/pixel
	ESP[a]	0.71-0.75 ms	0.95-0.99 ms	1.02-1.10 ms
	BW_y[a]	24.7-26.1 Hz/pixel	21.0-21.9 Hz/pixel	20.2-21.8 Hz/pixel
	TR[a]	52.8-53.9 ms	58.3-59.5 ms	58.8-60.4 ms
	N_{vol}	55 (1-5 removed for tSNR)	45 (1-3 removed for tSNR)	35 (1-2 removed for tSNR)
	Figure 2	A	B	C

BW_x, readout bandwidth; BW_y, phase encode bandwidth; EF, EPI factor; ESP, echo spacing; $N_{shots} = S\cdot N_{slices}/R_z$, number of shots per volume measurement; N_{slices}, number of slices; N_{vol}, number of volume measurements; Res., resolution; TR_{vol}, acquisition time per volume measurement; tSNR, temporal SNR.

[a] ESP varies at constant BW_x due to varying z-blip durations (varying ramp sampling).

TABLE 2 Sampling trajectories and sequence parameters for structural EPI acquisitions using large y-blips

	y-blip 21, 22, 21	y-blip 30	y-blip 30, 20, 10
	CAIPI sampling trajectory (TR_{vol} / TA)		
Skipped	$21\cdot1\times2_{z1}$ (26 s/0:31)	$30\cdot1\times5_{z2}$ (30.0 s/0:44)	$15\cdot2\times2_{z1}$ (37.5 s/0:52-2:44[a])
	$11\cdot2\times2_{z1}$ (14 s/0:19)	$10\cdot3\times2_{z1}$ (25.0 s/0:39)	$10\cdot2\times2_{z1}$ (31.0 s/0:45)
	$7\cdot3\times2_{z1}$ (10 s/0:14)	$30\cdot1\times7_{z3}$ (21.0 s/0:35)	$5\cdot2\times2_{z1}$ (24.5 s/0:39)
EF	7	9	9, 14, 27
Res.	1.2 mm isotropic	0.8 mm isotropic	0.8 mm isotropic
Matrix	192 × 192	270 × 270	270 × 270
FOV	230 mm × 230 mm	216 mm × 216 mm	216 mm × 216 mm
N_{slices}	160	200 (196 for R = 7)	200
P. Fourier	6/8 × 1	1 × 1	1 × 1
TE	4.35 ms	10 ms	10.0, 12.8, 22.2 ms
TR	15.7 ms	25 ms	25, 31, 48 ms
BW_x	1184 Hz/pixel	806 Hz/pixel	806 Hz/pixel
ESP	1.07, 1.09, 1.07 ms	1.55 ms	1.55, 1.51, 1.46 ms
BW_y	102.2, 105.1, 102.2 Hz/pixel	71.7 Hz/pixel	71.7, 49.1, 25.3 Hz/pixel
ACS	48 × 16	48 × 48	48 × 48
T_{pre} in TA	4.9 s	13.9 s	13.9 s
Figure 3	A	B	C, D[a]

ACS, autocalibration scan (y × z matrix); P. Fourier, partial Fourier factor; TA, total acquisition time including multiple volume measurements and preparation time; T_{pre}, preparation time (external phase correction + autocalibration scan dummy shots + FLASH autocalibration scan dummy shots); TR, repetition time per shot; TR_{vol}, acquisition time per volume measurement.

[a] N_{vol} = 4 volume measurements.

3.2.1 | Functional MRI protocol type

Time series data were acquired with 26 different protocols according to Table 1 using oblique axial slice orientation. In terms of temporal SNR (tSNR), the selected protocols corresponded to the best applicable blipped-, shot-selective, and skipped-CAIPI trajectories with $4 \le R \le 8$. Because *ESP* increases with resolution, decreasing *EF*s of 54, 48, and 45 were necessary to achieve TE = 30 ms, which corresponds to *y*-blips 2, 3, and 4. A 15° binomial-121 water excitation pulse was employed to maximize gray matter signal (sinc, bandwidth time product = 30, slab scaled to 90% of nominal slice FOV). Between each excitation and EPI readout, a standard integrated phase correction scan was acquired.

3.2.2 | Dual-polarity autocalibration scan

As part of each time series acquisition, 48 × 48 initial autocalibration scan lines prepared by 200 steady-state dummy shots were acquired using a $\left(S\cdot R_y\right)\cdot1\times1_{z0}$ segmented EPI sampling (BW_y matched to subsequent imaging) with minimal TE and TR (Figure 1D). Every shot was acquired twice with alternating readout polarity, each echo phase corrected (almost ghost-free) and then complex averaged (completely ghost-free). This simplified dual-polarity autocalibration scan corresponds to the first steps of dual-polarity GRAPPA processing[42] and integrates easily without reconstruction customization.

3.2.3 | Structural MRI protocol type

All structural scans according to Table 2 used sagittal slice orientation (readout: head-feet). All EPI scans employed a single hard pulse excitation set to approximately 2.4 ms duration for water excitation at 3 Tesla.[6,43] A single external phase correction scan (5° excitation), followed by 100 FLASH dummy shots and autocalibration scan lines,[44] were acquired as a prescan (Figure 1E). The total duration, T_{pre}, was included in all stated TAs.

For submillimeter scans, TR = 25 ms and a flip angle (FA) of 30° were used. Four volumes were acquired using a $15\cdot2\times2_{z1}$ sampling for retrospective averaging with anteroposterior primary phase encode direction. The scan was repeated once with inverted phase encode direction (posteroanterior). As an EPI factor-free reference, the

vendor-provided 3D multi-echo (ME) FLASH sequence, lacking CAIPIRINHA sampling, was used with otherwise identical parameters, except for a slightly altered FOV (230 mm along readout, 192 slices), 0.1 ms hard pulse excitation, and readout $BW_x = 380$ Hz/pixel for each of 6 bipolar echoes (TE $\in$ [3.8,19.3]ms). The resulting TA = 5:36 approximates the combined duration of anteroposterior and posteroanterior EPI scans with 4 averages each (5:28).

Additional TR/TE/FA/*EF*-matched EPIs with alternative CAIPI patterns were acquired. Furthermore, the $2 \times 2_{z1}$ pattern was sampled with varying segmentation factors, $S = 15$, 10, and 5. Finally, 1.2 mm isotropic data were acquired, adapting and extending a rapid T_1-weighted scan recently proposed for clinical use[6]: for consistent TR = 15.7 ms and TE = 4.35 ms across different CAIPI patterns, $EF = 7$ and minimal sequence dead times and shots per measurement were maintained by adjusting S, as facilitated by skipped-CAIPI (Table 2).

3.2.4 | Processing

All processing was performed using the FMRIB Software Library[45] and Python. Time series were preprocessed using FEAT, including temporal high-pass filtering (100 s) and motion correction. 5, 3, or 2 initial volumes were discarded before computing voxel-wise tSNR, finally divided by $\sqrt{TR_{vol}}$ to assess tSNR efficiency.

The combined 8 volumes of the anatomical anteroposterior and posteroanterior $15 \cdot 2 \times 2_{z1}$ scans were processed using TOPUP to estimate and correct for motion and geometric distortions. The corrected magnitude images were averaged for visual comparison to the ME-FLASH image. For the latter, all TE magnitude images were averaged for maximal SNR and comparable T_2^*-weighting.

4 | RESULTS

Figure 2 shows a sagittal example view of the best time series tSNR and efficiency results for $R = 4$, 5, 6, 7, and 8 at isotropic resolutions of 2 mm (A), 1.5 mm (B), and 1.2 mm (C). The respective volume TRs and the quartiles of the whole-brain tSNR efficiencies are printed above and below the maps, respectively. Results of the alternative protocols according to Table 1, for which the CAIPI pattern resulted in minor-to-major efficiency degradation for the same R, are shown in Supporting Information Figure S6.

The first three columns of Figure 3 show axial example views of single volume T_1-weighted EPI scans at 1.2 mm isotropic resolution according to Ref. 6, with varying CAIPI patterns and constant $EF = 7$ (A), and at 0.8 mm isotropic resolution with varying CAIPI patterns and constant $EF = 9$ (B), and with varying EF and constant $2 \times 2_{z1}$ CAIPI pattern (C). The two rightmost columns show corresponding views and magnified zooms following magnitude averaging (D, from top to bottom): 4 volumes, 8 volumes following motion and distortion correction, and 6 TEs of the FA/TR/TA-matched ME-FLASH. Yellow arrows indicate the effect of distortion correction. Supporting Information Figure S7 shows corresponding orthogonal views and additional examples with local SNR estimates and an MP-RAGE scan for anatomical reference. Supporting Information Figure S8 shows the actual k-space samplings used.

5 | DISCUSSION

Previous blipped-CAIPI and shot-selective CAIPI approaches corresponded to exactly 2 possible EPI trajectories given a specific CAIPI pattern. By implication, instead of selecting the optimal CAIPI pattern, it often had to be selected according to the associated y-blip that fit the matrix size, TE, TR, or EF prerequisites, in particular at high temporal resolution applications such as fMRI. Large y-blips for high spatial resolution with minimal geometric distortions require segmentation, which previously only provided limited CAIPI options without z-blips. In both resolution domains, skipped-CAIPI increases protocol flexibility without compromising controlled aliasing quality. In fact, by selecting a g-factor-optimal CAIPI pattern first, and then selecting a segmentation factor to adjust EF or BW_y via the y-blip, chances are relatively high ($1{:}n_1$) to yield a trajectory without z-blips but $n_1 - 1$ times higher to yield a trajectory with z-blips (Supporting Information Figures S1-S2). From this point of view, skipped-CAIPI may as well be understood as segmented EPI with a CAIPI shift. This implies all pros and cons of the utility of segmented EPI. The segmentation factor blends between the special cases of blipped-CAIPI ($S = 1$), shot-selective CAIPI ($S = n_1$), and skipped-CAIPI without z-blips ($S = 2n_1, 3n_1, \ldots$).

The resulting flexibility is demonstrated by the T_1-weighted 3D-EPI examples of Figure 3, where one parameter was varied while others were kept fix without introducing unnecessary sequence dead times, as facilitated by skipped-CAIPI. FLASH-like acquisitions with sufficient contrast-to-noise ratio (eg, 1.2 mm data, A) can be used for rapid MR parameter quantification,[10,46-48] and they also have great clinical potential as a rapid structural imaging alternative,[6] especially if extended to other contrasts.[4,49] At 7 Tesla, an established method for efficient high-resolution T_2^*/susceptibility-weighted imaging uses segmented 3D-EPI without CAIPI sampling.[1] In this example, skipped-CAIPI could either reduce the g-factor at unchanged undersampling factor of 2 or accelerate further with negligible

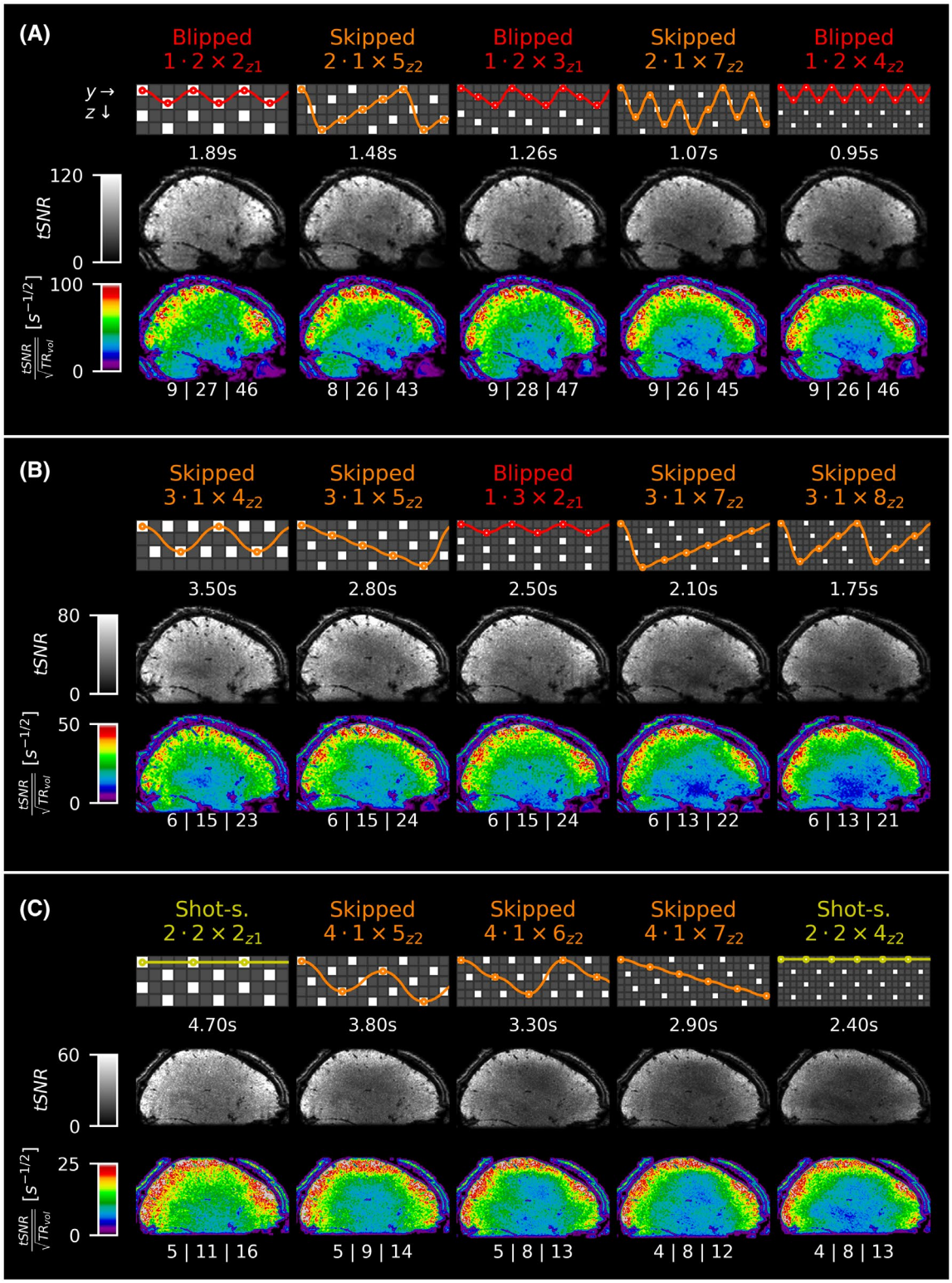

FIGURE 2 Temporal SNR maps and tSNR efficiency maps for the time series data acquired with different CAIPI patterns resulting in $R = 4 - 8$ (from left to right), which provided the best overall tSNR efficiency at 2.0 mm (A, *y*-blip 2), 1.5 mm (B, *y*-blip 3), and 1.2 mm isotropic resolution (C, *y*-blip 4) under the described experimental conditions. Out of 15 presented cases, 9 were not applicable previously ("skipped"). The respective CAIPI pattern, along with 1 example trajectory and TR_{vol}, is indicated above each tSNR map. Whole-brain tSNR efficiency quartiles are indicated below the maps. For the remaining, second- to third-best results according to alternative CAIPI scans of Table 1, as well as example magnitude images, see Supporting Information Figure S6. tSNR, temporal SNR

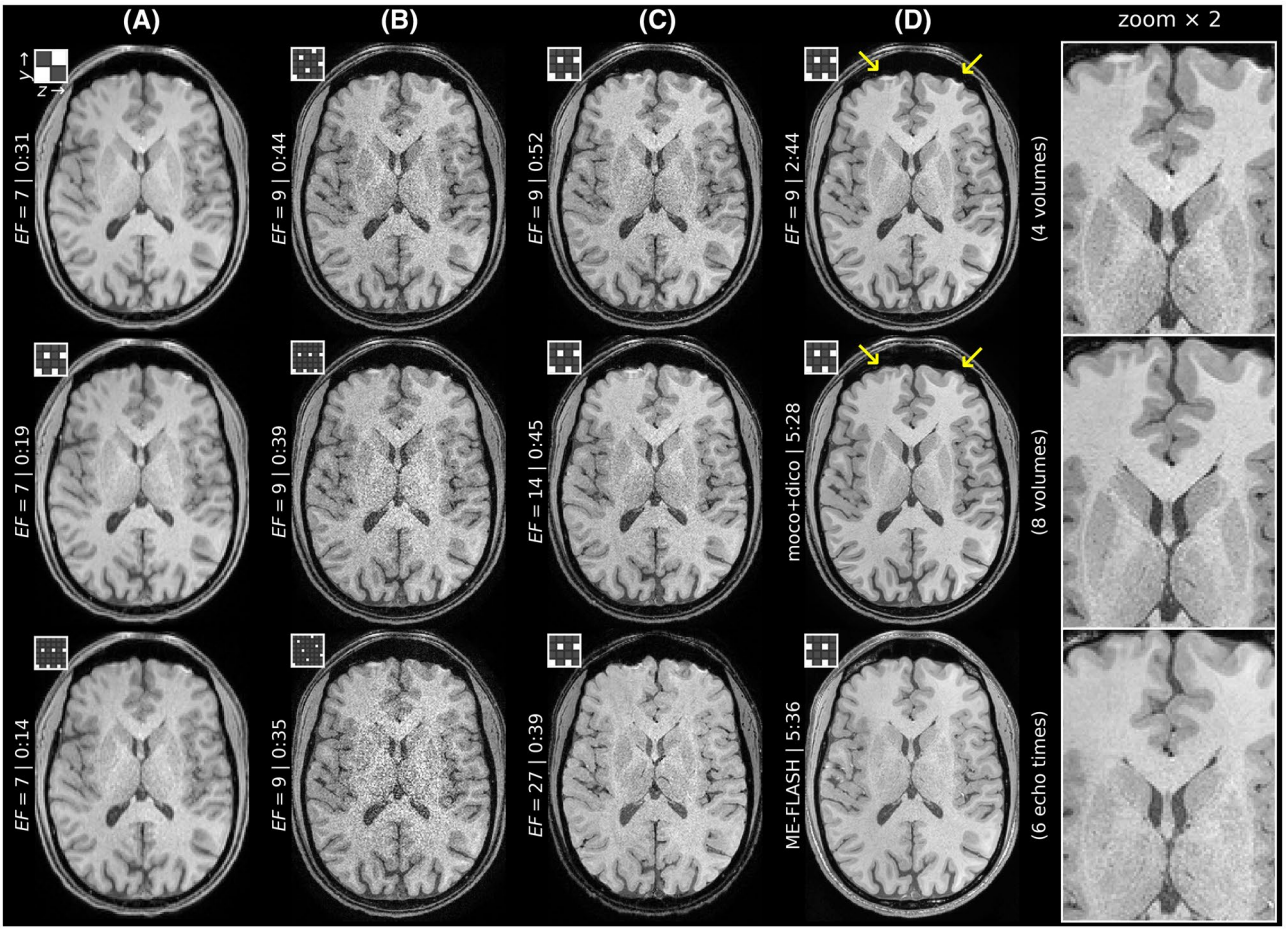

FIGURE 3 Axial example slice of several rapid T_1-weighted high-resolution whole-head scans (TA stated in [min:s]) along with the respective elementary CAIPIRINHA sampling cells.[37] (A) 1.2 mm isotropic protocols adapted from Ref. 6 (row 1), with increasing CAIPI undersampling while keeping $EF = 7$ constant. (B-D) 0.8 mm isotropic protocols with increasing CAIPI undersampling while keeping $EF = 7$ constant (B), with increasing *EF* while keeping CAIPI pattern constant (C), and four- and eightfold magnitude-average without and with correction for motion and geometric distortions compared to the echo-average of a TR- and TA-matched ME-FLASH (D). See Supporting Information Figure S7 for orthogonal example slices of (D), additional scan comparisons, and local SNR estimates. See Supporting Information Figure S8 for complete k-space sampling of scans (A-C). dico, distortion correction; EF, EPI factor; ME-FLASH, multi-echo FLASH; moco, motion correction

g-factor increase. Either way, TE, TR, and *EF* could be left unchanged. Reduced intravolume motion sensitivity, as single measurements get faster, and the option of intervolume correction for motion and distortion before averaging pose a general advantage over a single 3D-(ME)-FLASH scan of the same total acquisition and spatial coverage. This is demonstrated by Figure 3D and Supporting Information Figure S7. Although the subject was instructed to lie still, the eightfold EPI average even shows sharper image details at similar SNR. The same level of motion-robustness can be achieved with traditional segmented 3D-EPI, however, without the benefit of controlled aliasing. More SNR may be gained if corrections (including voxel-wise phase drift) and averaging are performed on the complex images. In terms of SNR, complex image averaging is equivalent to k-space oversampling (or extended slab coverage[1]) as long as the g-factor is negligible. Therefore, the ability to acquire faster without reducing SNR efficiency (eg, EPI vs. FLASH) or to increase SNR without slowing down acquisition (eg, segmented EPI with CAIPI vs. without CAIPI) reflects 1 strength of skipped-CAIPI.

Aside from high-resolution imaging, skipped-CAIPI is also beneficial, if smaller *y*-blips are required, for example for fMRI. According to Supporting Information Figures S3-S5, even with small *y*-blips the majority of CAIPI patterns could previously not be sampled by means of EPI. For several blipped-, shot-selective, and skipped-CAIPI trajectories, the combined effect of *g*, *R*, receive sensitivity, physiological noise,[50] and temporal resolution was assessed by tSNR and tSNR efficiency. The free choice of CAIPI pattern, independent of the required *y*-blip, has demonstrated maximum efficiency across previously inaccessible undersampling factors and resolutions (Figure 2). For instance, *y*-blip 3 scans can now additionally be acquired using well-suitable $R = 2, 4^*, 5^*, 7^*, 8^*, 10, \ldots$ CAIPI patterns compared to previously only $R = 3, 6^*, 9, \ldots$. (*demonstrated here).

Note: which CAIPI pattern is optimal may differ when using a different array coil, slice orientation. or slice coverage. A limitation of any EPI sampling is that the *y*-blip is a multiple of R_y. For instance, the $2\times2_{z1}$ CAIPI pattern used for the anatomical protocol (*y*-blip 30) could not be used for the 1.5 mm functional protocol (*y*-blip 3). On the other hand, $R_y = 1$ skipped-CAIPI trajectories, such as $S\cdot1\times4_{z2}$, are generally applicable and can be beneficial in terms of g-factor. Therefore, filling gaps of previously inaccessible undersampling options with minimal g-factor penalty reflects another strength of skipped-CAIPI.

Although skipped-CAIPI has been discussed for the 2D phase encoding space of 3D-EPI, it can just as well be applied to the SMS-3D sampling space.[38,39] Shot-selective CAIPI, for instance, has already been used with SMS-EPI for dynamic contrast-enhanced imaging.[5] This implementation could be adopted for skipped-CAIPI sampling either without *z*-blips or with *z*-blips. A skipped-CAIPI SMS option may be advantageous for certain applications or physiological noise versus thermal noise regimes.[51] However, the limitations of traditional segmented EPI compared to single-shot EPI, that is, an increased sensitivity to shot-to-shot signal variations, also apply to SMS-EPI using skipped-CAIPI or shot-selective CAIPI sampling. On the other hand, high-resolution MRI, which may benefit most from skipped-CAIPI sampling, also benefits most from volumetric (3D) imaging.[33,52] For multi-echo fMRI[53-56] or ultrahigh-field fMRI, where often partial Fourier sampling and large R_y are employed to minimize *EF*, TE, and geometric distortions, alternative skipped-CAIPI sampling is valuable, in particular with high-density receive arrays[13,18] or for laminar resolution imaging.[57,58] Furthermore, eased matching of the phase encode bandwidth between scans with different matrix sizes or CAIPI patterns fosters rapid, distortion-matched high-contrast acquisitions,[19,59,60] even at resolutions differing from the corresponding functional scan.

6 | CONCLUSION

Introducing segmentation into blipped-CAIPI, or equivalently, introducing a CAIPI shift into segmented EPI, allows to select a g-factor-optimal 2D CAIPIRINHA pattern and the primary phase encode gradient blip independently to adjust geometric distortions, TEs, TRs, and so forth. Almost arbitrary EPI factors combined with minimal parallel imaging noise are thus made available to numerous MR imaging methods, including volumetric high-resolution imaging. Although the implementation is simple, the versatility gain of typical and nontypical applications of 3D-EPI or SMS-EPI can be vast. The authors are open to share 3D-EPI pulse sequence binaries featuring skipped-CAIPI via C2P procedure (Siemens Healthineers). An interactive Jupyter Notebook to reproduce skipped-CAIPI trajectories is made available at https://github.com/mrphysics-bonn/skipped-caipi.

ACKNOWLEDGMENT

Open access funding enabled and organized by Projekt DEAL.

ORCID

Rüdiger Stirnberg https://orcid.org/0000-0001-7021-1063
Tony Stöcker https://orcid.org/0000-0002-8946-9141

REFERENCES

1. Zwanenburg JJ, Versluis MJ, Luijten PR, Petridou N. Fast high resolution whole brain T2* weighted imaging using echo planar imaging at 7T. *Neuroimage*. 2011;56:1902-1907.
2. Sati P, Thomasson DM, Li N, et al. Rapid, high-resolution, whole-brain, susceptibility-based MRI of multiple sclerosis. *Mult Scler*. 2014;20:1464-1470.
3. Falkovskiy P, Brenner D, Feiweier T, et al. Comparison of accelerated T1-weighted whole-brain structural-imaging protocols. *Neuroimage*. 2016;124:157-167.
4. Skare S, Sprenger T, Norbeck O, et al. A 1-minute full brain MR exam using a multicontrast EPI sequence. *Magn Reson Med*. 2018;79:3045-3054.
5. Eickel K, Porter DA, Söhner A, Maaß M, Lüdemann L, Günther M. Simultaneous multislice acquisition with multi-contrast segmented EPI for separation of signal contributions in dynamic contrast-enhanced imaging. *PLoS One*. 2018;13:e0202673.
6. Norbeck O, Sprenger T, Avventi E, et al. Optimizing 3D EPI for rapid T1-weighted imaging. *Magn Reson Med*. 2020;84:1441-1455.
7. Sun H, Wilman AH. Quantitative susceptibility mapping using single-shot echo-planar imaging. *Magn Reson Med*. 2015;73:1932-1938.
8. Langkammer C, Bredies K, Poser BA, et al. Fast quantitative susceptibility mapping using 3D EPI and total generalized variation. *Neuroimage*. 2015;111:622-630.
9. Stirnberg R, Deistung A, Reichenbach J, Stöcker T. Accelerated quantitative susceptibility and R2* mapping with flexible k-t-segmented 3D-EPI. In Proceedings of the 26th Annual Meeting of ISMRM, Paris, France, 2018. Abstract 0320.
10. Wang D, Stöcker T, Stirnberg R. Fast quantitative multiparametric mapping using 3D-EPI with segmented CAIPIRINHA sampling at 3T. In Proceedings of the ISMRM & SMRT Virtual Conference & Exhibition, Sydney, Australia, 2020. Abstract 0565.
11. Smith SM, Beckmann CF, Andersson J, et al. Resting-state fMRI in the human connectome project. *Neuroimage*. 2013;80:144-168.
12. Lutti A, Thomas DL, Hutton C, Weiskopf N. High-resolution functional MRI at 3 T: 3D/2D echo-planar imaging with optimized physiological noise correction. *Magn Reson Med*. 2013;69:1657-1664.
13. Petridou N, Italiaander M, van de Bank BL, Siero JCW, Luijten PR, Klomp DWJ. Pushing the limits of high-resolution functional MRI using a simple high-density multi-element coil design. *NMR Biomed*. 2013;26:65-73.
14. Batson MA, Petridou N, Klomp DW, Frens MA, Neggers SF. Single session imaging of cerebellum at 7 Tesla: Obtaining structure and function of multiple motor subsystems in individual subjects. *PLoS One*. 2015;10:e0134933.

15. Goncalves NR, Ban H, Sánchez-Panchuelo RM, Francis ST, Schluppeck D, Welchman AE. 7 Tesla fMRI reveals systematic functional organization for binocular disparity in dorsal visual cortex. *J Neurosci*. 2015;35:3056-3072.
16. Stirnberg R, Huijbers W, Brenner D, Poser BA, Breteler M, Stöcker T. Rapid whole-brain resting-state fMRI at 3 Tesla: Efficiency-optimized three-dimensional EPI versus repetition time-matched simultaneous-multi-slice EPI. *Neuroimage*. 2017;163:81-92.
17. Fracasso A, Luijten PR, Dumoulin SO, Petridou N. Laminar imaging of positive and negative BOLD in human visual cortex at 7 T. *Neuroimage*. 2018;164:100-111.
18. Hendriks AD, D'Agata F, Raimondo L, et al. Pushing functional MRI spatial and temporal resolution further: High-density receive arrays combined with shot-selective 2D CAIPIRINHA for 3D echo-planar imaging at 7 T. *NMR Biomed*. 2020;33:e4281.
19. van der Zwaag W, Buur PF, Fracasso A, et al. Distortion-matched T1 maps and unbiased T1-weighted images as anatomical reference for high-resolution fMRI. *Neuroimage*. 2018;176:41-55.
20. van der Zwaag W, Reynaud O, Narsude M, Gallichan D, Marques JP. High spatio-temporal resolution in functional MRI with 3D echo planar imaging using cylindrical excitation and a CAIPIRINHA undersampling pattern. *Magn Reson Med*. 2018;79:2589-2596.
21. Le Ster C, Moreno A, Mauconduit F, et al. Comparison of SMS-EPI and 3D-EPI at 7T in an fMRI localizer study with matched spatiotemporal resolution and homogenized excitation profiles. *PLoS One*. 2019;14:e0225286.
22. Mansfield P. Mutli-planar image formation using NMR spin echoes. *J Phys C: Solid State Phys*. 1977;10:L55-L58.
23. Brunner P, Ernst RR. Sensitivity and performance time in NMR imaging. *J Magn Reson (1969)*. 1979;33:83-106.
24. Deichmann R, Adolf H, Nöth U, Kuchenbrod E, Schwarzbauer C, Haase A. Calculation of signal intensities in hybrid sequences for fast NMR imaging. *Magn Reson Med*. 1995;34:481-489.
25. Breuer FA, Blaimer M, Heidemann RM, Mueller MF, Griswold MA, Jakob PM. Controlled aliasing in parallel imaging results in higher acceleration (CAIPIRINHA) for multi-slice imaging. *Magn Reson Med*. 2005;53:684-691.
26. Pruessmann KP, Weiger M, Scheidegger MB, Boesiger P. SENSE: Sensitivity encoding for fast MRI. *Magn Reson Med*. 1999;42:952-962.
27. Setsompop K, Gagoski BA, Polimeni JR, Witzel T, Wedeen VJ, Wald LL. Blipped-controlled aliasing in parallel imaging for simultaneous multislice echo planar imaging with reduced g-factor penalty. *Magn Reson Med*. 2012;67:1210-1224.
28. Poser B, Kemper V, Ivanov D, Kannengiesser S, Uludağ K, Barth M. CAIPIRINHA-accelerated 3D EPI for high temporal and/or spatial resolution EPI acquisitions. In Proceedings of the European Society for Magnetic Resonance in Medicine and Biology 2013 Congress, Toulouse, France, 2013. p. 151-301.
29. Poser BA, Ivanov D, Kannengiesser SA, Uludağ K, Barth M. Accelerated 3D EPI using 2D blipped-CAIPI for high temporal and/or spatial resolution. In Proceedings of the 22nd Annual Meeting of ISMRM, Milan, Italy, 2014. p. 1506.
30. McKinnon GC. Ultrafast interleaved gradient-echo-planar imaging on a standard scanner. *Magn Reson Med*. 1993;30:609-616.
31. Feinberg D, Oshio K. Phase errors in multi-shot echo planar imaging. *Magn Reson Med*. 1994;32:535-539.
32. Hennel F. Multiple-shot echo-planar imaging. *Concepts Magn Reson*. 1997;9:43-58.
33. Poser B, Koopmans P, Witzel T, Wald L, Barth M. Three dimensional echo-planar imaging at 7 Tesla. *Neuroimage*. 2010;51:261-266.
34. Narsude M, Marques JP, Gallichan D, Gruetter R. Superior GRAPPA reconstruction with reduced g-factor noise using 2D CAIPIRINHA for 3D EPI. In Proceedings of the 21st Annual Meeting of ISMRM, Salt Lake City, UT, 2013. p. 3705.
35. Narsude M, Gallichan D, Van Der Zwaag W, Gruetter R, Marques JP. Three-dimensional echo planar imaging with controlled aliasing: A sequence for high temporal resolution functional MRI. *Magn Reson Med*. 2016;75:2350-2361.
36. Reynaud O, Jorge J, Gruetter R, Marques JP, van der Zwaag W. Influence of physiological noise on accelerated 2D and 3D resting state functional MRI data at 7T. *Magn Reson Med*. 2017;78:888-896.
37. Breuer FA, Blaimer M, Mueller MF, et al. Controlled aliasing in volumetric parallel imaging (2D CAIPIRINHA). *Magn Reson Med*. 2006;55:549-556.
38. Zahneisen B, Poser BA, Ernst T, Stenger VA. Three-dimensional Fourier encoding of simultaneously excited slices: Generalized acquisition and reconstruction framework. *Magn Reson Med*. 2014;71:2071-2081.
39. Zahneisen B, Ernst T, Poser BA. SENSE and simultaneous multislice imaging. *Magn Reson Med*. 2015;74:1356-1362.
40. Poser BA, Setsompop K. Pulse sequences and parallel imaging for high spatiotemporal resolution MRI at ultra-high field. *Neuroimage*. 2018;168:101-118.
41. Griswold MA, Jakob PM, Heidemann RM, et al. Generalized autocalibrating partially parallel acquisitions (GRAPPA). *Magn Reson Med*. 2002;47:1202-1210.
42. Hoge WS, Polimeni JR. Dual-polarity GRAPPA for simultaneous reconstruction and ghost correction of echo planar imaging data. *Magn Reson Med*. 2016;76:32-44.
43. Stirnberg R, Brenner D, Stöcker T, Shah NJ. Rapid fat suppression for three-dimensional echo planar imaging with minimized specific absorption rate. *Magn Reson Med*. 2016;76:1517-1523.
44. Ivanov D, Barth M, Uludağ K, Poser BA. Robust ACS acquisition for 3D echo planar imaging. In Proceedings of the 23rd Annual Meeting of ISMRM, Toronto, Ontario, Canada, 2015. p. 2059.
45. Jenkinson M, Beckmann CF, Behrens TEJ, Woolrich MW, Smith SM. Fsl. *Neuroimage*. 2012;62:782-790.
46. Christensen KA, Grant DM, Schulman EM, Walling C. Optimal determination of relaxation times of Fourier transform nuclear magnetic resonance. Determination of spin-lattice relaxation times in chemically polarized species. *J Phys Chem*. 1974;78:1971-1976.
47. Helms G, Dathe H, Dechent P. Quantitative FLASH MRI at 3T using a rational approximation of the Ernst equation. *Magn Reson Med*. 2008;59:667-672.
48. Weiskopf N, Suckling J, Williams G, et al. Quantitative multiparameter mapping of R1, PD*, MT, and R2* at 3T: A multi-center validation. *Front Neurosci*. 2013;7:95.
49. Sprenger T, Norbeck O, Berglund J, Avventi E, Skare S. EPIMix 3.0. In Proceedings of the 27th Annual Meeting of ISMRM, Montréal, Québec, Canada, 2019. p. 1190.
50. Triantafyllou C, Hoge RD, Krueger G, et al. Comparison of physiological noise at 1.5 T, 3 T and 7 T and optimization of fMRI acquisition parameters. *Neuroimage*. 2005;26:243-250.

51. van der Zwaag W, Marques JP, Kober T, Glover G, Gruetter R, Krueger G. Temporal SNR characteristics in segmented 3D-EPI at 7T. *Magn Reson Med*. 2012;67:344-352.
52. Marques JP, Norris DG. How to choose the right MR sequence for your research question at 7 T and above? *Neuroimage*. 2018;168:119-140.
53. Posse S, Wiese S, Gembris D, et al. Enhancement of BOLD-contrast sensitivity by single-shot multi-echo functional MR imaging. *Magn Reson Med*. 1999;42:87-97.
54. Poser BA, Norris DG. Investigating the benefits of multi-echo EPI for fMRI at 7 T. *Neuroimage*. 2009;45:1162-1172.
55. Kundu P, Voon V, Balchandani P, Lombardo MV, Poser BA, Bandettini PA. Multi-echo fMRI: A review of applications in fMRI denoising and analysis of BOLD signals. *Neuroimage*. 2017;154:59-80.
56. Puckett AM, Bollmann S, Poser BA, Palmer J, Barth M, Cunnington R. Using multi-echo simultaneous multi-slice (SMS) EPI to improve functional MRI of the subcortical nuclei of the basal ganglia at ultra-high field (7T). *Neuroimage*. 2018;172:886-895.
57. Huber L, Ivanov D, Handwerker DA, et al. Techniques for blood volume fMRI with VASO: From low-resolution mapping towards sub-millimeter layer-dependent applications. *Neuroimage*. 2018;164:131-143.
58. Huber L, Chai Y, Stirnberg R, et al. Beyond the limits of layer-dependent CBV fMRI in humans: Strategies towards whole brain coverage, sub-second TR, and very high 0.5mm resolutions. In Proceedings of the ISMRM & SMRT Virtual Conference & Exhibition, Sydney, Australia, 2020. Abstract 3864.
59. Renvall V, Witzel T, Wald LL, Polimeni JR. Automatic cortical surface reconstruction of high-resolution T1 echo planar imaging data. *Neuroimage*. 2016;134:338-354.
60. Kashyap S, Ivanov D, Havlicek M, Poser BA, Uludağ K. Impact of acquisition and analysis strategies on cortical depth-dependent fMRI. *Neuroimage*. 2018;168:332-344.

SUPPORTING INFORMATION

Additional Supporting Information may be found online in the Supporting Information section.

FIGURE S1 EPI factors (EF) as a result of segmentation when combining a relatively small ($N_y = 108$) and large ($N_y = 270$) phase encode matrix size with three different CAIPI pattern examples. The phase encode bandwidth is proportional to the y-blip (horizontal axis). A/B: logarithmic/linear EF axis (according to a reduced range of segmentation factors indicated by dotted rectangle in A). Using traditional segmented EPI (blue line: same undersampling pattern, but without CAIPI shift), a wide range of EPI factors and y-blips is applicable. Blipped-CAIPI and shot-selective CAIPI only correspond to two distinct EPI factors and y-blips. With skipped-CAIPI, all EPI factors and y-blips of segmented EPI can be applied with a reduced g-factor. Vertical grid lines in B indicate EPI trajectories without z-blips ($S = n_1, 2n_1, 3n_1, \ldots$, where n_1: blipped-CAIPI z-blip cycle). Inset displays in B show the respective blipped-CAIPI and shot-selective CAIPI trajectories and the first unique skipped-CAIPI option (phase encoding trajectory of the first shot: thick, bright curve; phase encoding trajectories of subsequent shots: thinner, darker curves). Each white rectangle corresponds to a frequency-encoded echo readout (x perpendicular to the paper plane)

FIGURE S2 Z-blips and z-blip cycles of various CAIPI trajectories for the example patterns of S1. For the sake of generality, $\Delta z \in \mathbb{Z}$ (see Appendix). Both trajectories for negative and positive CAIPI shifts are indicated on the example of the first of S shots. Identical z-blips/cycle apply to all following shots (albeit starting at a different offset in the cycle). Identical z-blips/cycle also occur for the same CAIPI pattern with segmentation factors $S' = S, S + n_1, S + 2n_1, \ldots$, whereby n_1 denotes the blipped-CAIPI z-blip cycle ($S = 1$) associated to the CAIPI pattern

FIGURE S3 Applicable and not applicable EPI $R \leq 8$ undersampling according to (37) with a fixed y-blip $S \cdot R_y = 2$. Only $\Delta_z \geq 0$ patterns are plotted, but corresponding $-\Delta_z$ patterns are counted (±). First trajectory/subsequent trajectories indicated by thick and bright/thinner and darker curves. Sampling trajectories used for experimental time series acquisition in this work indicated by $*$ (cf. Table 1, Figure 2, Supporting Information Figure S6)

FIGURE S4 Same as S3 with fixed y-blip $S \cdot R_y = 3$.

FIGURE S5 Same as S3 with fixed y-blip $S \cdot R_y = 4$. The $R = 2,4,6,8$ skipped-CAIPI schemes include trajectories without z-blips

FIGURE S6 Temporal SNR and tSNR efficiency maps of second-to-third best time series data acquired in this work. Even though these were the best applicable blipped-CAIPI, shot-selective CAIPI and skipped-CAIPI trajectories for the respective total undersampling factors at fixed y-blips of 2 (A, 2 mm isotropic), 3 (B, 1.5 mm isotropic) and 4 (C, 1.2 mm isotropic), the corresponding CAIPI patterns lead to marginally-to-substantially worse results than the optimal CAIPI patterns shown in Figure 2. For instance, skipped-CAIPI $2 \cdot 1 \times 6_{z2}$ performed only marginally worse than the optimal blipped-CAIPI $1 \cdot 2 \times 3_{z1}$ trajectory (cf. Figure 2). The $1 \times 6_{z3}$ CAIPI pattern performed particularly poorly, irrespective of the trajectory used (cf. A,B). However, the performance may differ using a different coil, slice coverage or slice orientation. The enlarged views on the right show the mean magnitude images of the respective $R = 8$ skipped-CAIPI acquisition. The 1.5 mm example is also shown without automatic receive sensitivity correction ("prescan normalize") to indicate the receive sensitivity

FIGURE S7 Orthogonal example slices of T_1-weighted high-resolution whole-head scans (TA stated in [min:s]) corresponding to the axial slices shown in Figure 3D and three additional examples (right panel). Eight magnitude-averages of the $15 \cdot 2 \times 2_{z1}$ EPI scan (B) show improved anatomical accuracy due to motion and distortion

correction (moco+dico, yellow arrows) compared to four averages without corrections (A), and even improved resolution of details compared to the echo-average of a TR/FA/TA-matched ME-FLASH (C, red arrows). *A single-echo (TE = 3.8 ms) FLASH scan obtain with reduced TR = 12 ms and FA = 20° but otherwise identical parameters (D) and two magnitude-averages of the $\mathbf{15 \cdot 2 \times 2_{z1}}$ EPI following moco+dico (E) are additionally shown. Detailed views with a zoom factor of two are shown below all example slices. Blue numbers indicate rough SNR estimates from squared white matter regions indicated in the zoomed axial view of the corresponding MP-RAGE (F, 0.9 mm isotropic, 240 mm × 240 mm FOV, 192 slices, TE = 2.32 ms, TR = 2.3 s, TI = 900 ms, flip angle 8°, $\mathbf{2 \times 1}$ GRAPPA, 24 integrated ACS lines, TA = 5:21)

FIGURE S8 Visualization of the skipped-CAIPI samplings used for high-resolution T_1-weighted 3D-EPI scans in this work (cf. Table 2, Figure 3, Supporting Information Figure S7) along with the trajectory that covers the k-space center echo. Three out of nine examples shown follow a skipped-CAIPI EPI trajectory without *z*-blips ($\mathbf{10 \cdot 1 \times 5_{z2}}$, $\mathbf{10 \cdot 3 \times 2_{z1}}$, $\mathbf{10 \cdot 2 \times 2_{z1}}$). Complete and zoomed k-space views use the echo number ("Echoes") and the actual echo time ("Echo times (zoom)") for color-coding, respectively. Without echo time shifting (delaying the start time of each EPI trajectory by a fraction of the echo spacing according to the first primary phase encode value of the EPI trajectory, cf. Figure 1), the echo times color-coding would resemble the step-like echoes color-coding. Image artifacts would arise, where local magnetic field inhomogeneities are strong. However, due to echo time shifting, the echo times and the MR signal magnitude and phase at each frequency-encoded echo center evolve continuously along the primary phase encode direction.[31,32] As skipped-CAIPI can be understood as traditional segmented EPI with a CAIPI shift, this applies with or without CAIPI shift

How to cite this article: Stirnberg R, Stöcker T. Segmented K-space blipped-controlled aliasing in parallel imaging for high spatiotemporal resolution echo EPI. *Magn Reson Med*. 2021;85:1540–1551. https://doi.org/10.1002/mrm.28486

APPENDIX

Z-blips

The magnitudes of the two *z*-blips, $b_S^{(1)}$ and $b_S^{(2)}$, of any skipped-CAIPI trajectory are determined by $S \geq 1$ and the CAIPI parameters (in *z*-notation) $R_z > 1$ and $\Delta z \in \mathbb{Z}$:

$$\begin{aligned} b_S^{(1)} &= (S \cdot \Delta z) \mod R_z \\ b_S^{(2)} &= \left(R_z - b_S^{(1)}\right) \mod R_z \\ b_{S,min} &= min\left(b_S^{(1)}, b_S^{(2)}\right) \end{aligned} \tag{A1}$$

Here, mod denotes the remainder of the division operator (with the sign of the divisor).

Z-blip cycle

Every n_S echoes, the sequential *z*-blip order repeats:

$$n_S = \begin{cases} 1, & \text{if } b_{S,min} = b_S^{(1)} = b_S^{(2)} = 0 \\ R_z / b_{S,min}, & \text{if } R_z \mod b_{S,min} = 0 \\ R_z, & \text{else} \end{cases} \tag{A2}$$

The same *z*-blips/cycle apply for all segmentation factors $S' = S + m \cdot n_1 \geq 1$ with $m \in \mathbb{Z}$:

$$\begin{aligned} b_{S+m \cdot n_1}^{(1)} &= b_S^{(1)} \\ b_{S+m \cdot n_1}^{(2)} &= b_S^{(2)} \\ n_{S+m \cdot n_1} &= n_S \end{aligned} \tag{A3}$$

Here, n_1 is the blipped-CAIPI *z*-blip cycle. The special cases $S = n_1$ and $S' = 2n_1, 3n_1, \ldots$ imply no *z*-blips (cf. Supporting Information Figure S2).

Note: if $\Delta z \in \left[-\lfloor R_z/2 \rfloor, \lfloor R_z/2 \rfloor\right] \setminus \{0\}$, as assumed in this work, for blipped-CAIPI, Equation A2 simplifies to

$$n_1 = \begin{cases} R_z / |\Delta z|, & \text{if } R_z \mod \Delta z = 0 \\ R_z, & \text{else} \end{cases}. \tag{A4}$$